Dalton Transactions

PAPER

View Article Online
View Journal | View Issue

Cite this: *Dalton Trans.*, 2016, **45**, 9812

First-principles molecular dynamics simulation of the $Ca_2UO_2(CO_3)_3$ complex in water†

Chad Priest, Ziqi Tian and De-en Jiang*

Received 22nd November 2015,
Accepted 19th January 2016

DOI: 10.1039/c5dt04576b

www.rsc.org/dalton

Recent experiments have shown that the neutral $Ca_2UO_2(CO_3)_3$ complex is the dominant species of uranium in many uranyl-containing streams. However, the structure and solvation of such a species in water has not been investigated from first principles. Herein we present a first principles molecular dynamics perspective of the $Ca_2UO_2(CO_3)_3$ complex in water based on density functional theory and Born–Oppenheimer approximation. We find that the $Ca_2UO_2(CO_3)_3$ complex is very stable in our simulation timeframe for three different concentrations considered and that the key distances from our simulation are in good agreement with the experimental data from extended X-ray absorption fine structure (EXAFS) spectroscopy. More important, we find that the two Ca ions bind differently in the complex, as a result of the hydrogen-bonding network around the whole complex. This finding invites confirmation from time-resolved EXAFS and has implications in understanding the dissociative equilibrium of the $Ca_2UO_2(CO_3)_3$ complex in water.

Introduction

The concentration of uranium in seawater is very minute at about 3.3 ppb, but the large mass of seawater contains about 4.5 billion metric tons of uranium.[1] Mining uranium from seawater can provide an ideal sustainable alternative to current uranium mining methods (open pit, underground, and leaching) that create much environmental concern. In addition, extraction from seawater can provide a price ceiling for uranium that is of strategic importance in evaluating the economics of long-term supply of uranium for nuclear energy.[2,3]

Much research has been focused on the development of selective methods for mining uranium in seawater. Currently, the most viable method is utilizing an amidoxime-functionalized polymer sorbent known as poly(acrylamidoxime) fibers.[1–6] However, to make the uranium extraction from seawater economically viable, sorbent performance in terms of uranium uptake and uranium/vanadium selectivity needs to be further improved.[1,7] To design a better ligand and sorbent for uranium extraction, it is necessary to understand the fundamentals about uranium speciation in seawater.

In aqueous solution, uranium exists as the stable oxocation with an oxidation state of U(VI), called uranyl – UO_2^{2+}. Early work has focused on prying into the prominent equilibrium species bound to the uranyl complex in seawater[8] and suggested the anionic $[UO_2(CO_3)_3]^{4-}$ complex to be the dominant species in seawater. However, over the past two decades experimental data has shifted the consensus to cation-balanced complexes.[9–13] Concentrations of magnesium (Mg^{2+}) and calcium (Ca^{2+}) in seawater are overwhelmingly larger than the concentration of U(VI), so the ternary $Ca–UO_2–CO_3$ or $Mg–UO_2–CO_3$ exists predominately in seawater. The complexation of Ca^{2+} with $[UO_2(CO_3)_3]^{4-}$ has been validated experimentally by Bernhard *et al.*[10] and Kelly *et al.*[11] with extended X-ray absorption fine structure (EXAFS) spectroscopy. Most recently, Rao *et al.*[13] examined the thermodynamics of uranium in seawater and the complexation between Ca/Mg and $[UO_2(CO_3)_3]^{4-}$. They concluded that in seawater pH (8.2) $Ca_2UO_2(CO_3)_3$ accounts for 58% of the total uranium in the solution while $CaUO_2(CO_3)_3^{2-}$ and $MgUO_2(CO_3)_3^{2-}$ account for 18% each and $[UO_2(CO_3)_3]^{4-}$ accounts for only 6%.[13] In addition, Rao *et al.* studied the binding of U(VI) with various types of ligands and the subsequent leaching process.[14–19] In addition, the stability constant for the speciation of calcium is larger than magnesium.[13]

On the theoretical and computational side, work has been done on the binding of UO_2^{2+} with ligands using a cluster model[18,20–23] and on the structure and dynamics of $[UO_2(CO_3)_3]^{4-}$ in aqueous environment using molecular dynamics (MD) simulations.[24–27] Hofer *et al.* examined the structure and dynamics of $[UO_2(CO_3)_3]^{4-}$ in water using quantum mechanical charge field molecular dynamics (QMCF-MD).[24,25] Kerisit *et al.* investigated the structure and dynamics of $Ca_2UO_2(CO_3)_3$ in aqueous solution with classical MD simulations based on non-polarizable force fields.[26] Given

Department of Chemistry, University California, Riverside, California 92521, USA. E-mail: de-en.jiang@ucr.edu

†Electronic supplementary information (ESI) available. See DOI: 10.1039/c5dt04576b

the highly charged nature of Ca^{2+} ions and $[UO_2(CO_3)_3]^{4-}$, polarization may be important in describing the interaction between Ca^{2+} ions and $[UO_2(CO_3)_3]^{4-}$ and between the complex and the water molecules. First principles MD at the electronic structure would be desirable, as the polarization effect is taken into account automatically. However, no such work has been done on $Ca_2UO_2(CO_3)_3$ in aqueous solution, to the best of our knowledge.

The present work seeks to describe the structure and solvation of $Ca_2UO_2(CO_3)_3$ in water using first principles MD based on density functional theory (DFT-MD for short) for the first time. Our goal is to provide a fundamental baseline understanding of the structure and solvation of $Ca_2UO_2(CO_3)_3$ in water in terms of Ca–$UO_2(CO_3)_3$ and Ca–water interactions. The other goal is to compare DFT-MD simulations with the previous EXAFS data and classical MD simulations.

Computational methods

First-principles molecular dynamics simulations based on density functional theory (DFT-MD) and Born–Oppenheimer approximation were carried out using the Vienna *ab initio* simulation package with plane wave basis and periodic boundary conditions.[28,29] The Kohn–Sham equations are solved with the all-electron projected augmented wave (PAW) method.[30,31] We have chosen the Perdew–Burke–Ernzerhof (PBE) functional of the generalized-gradient approximation (GGA) for electron exchange and correlation.[32] PBE is one of the most popular GGA functionals, providing a balanced description for diverse molecules and materials, instead of being designed for a special class of molecules or interactions. In the case of liquid water, it has been shown that the PBE functional can describe well the peak positions in the radial distribution functions of g_{OO} and g_{OH} for the liquid structure of water but it overestimates the peak heights, in comparison with the experiment, leading to over-structuring.[33,34] Using hybrid functionals together with van der Waals interactions can soften the water structure, giving a better agreement with the experiment. But hybrid functionals are usually about two orders of magnitude more expensive than a pure DFT method such as GGA-PBE. We think that PBE is a reasonable choice in balancing accuracy and efficiency. In the ESI,† we provide an orbital-resolved local density of states for the U atom (Fig. S1†) from a snapshot of the $Ca_2UO_2(CO_3)_3$ complex in water to show that the bonding picture from the PBE functional is consistent with previous theoretical studies.[35,36]

The MD calculations were carried out at 298 K in a canonical NVT ensemble for a periodic cubic box that contains one $Ca_2UO_2(CO_3)_3$ complex in a fixed number of water molecules. Three concentrations were examined: 0.53 M, 0.42 M, and 0.36 M, corresponding to one $Ca_2UO_2(CO_3)_3$ complex in a periodic box containing 100, 125, and 150 water molecules, respectively; the corresponding simulation box sizes and densities are also compared in Table 1. Here we note that since there is only one complex in the simulation box for the three concentrations, this approach cannot probe the correlations between complexes but serves more to test the potential presence of size artifacts. We determined the densities from constant-pressure classical MD simulations using force-field parameters from a previous study.[26] The temperature was kept constant *via* a Nose–Hoover thermostat. A Verlet algorithm was used to integrate Newton's equation of motion with a time step of 1 femtosecond. After equilibration at 298 K for 15 ps, another 15 ps of production run was followed. Graphical visualization and analysis of the liquid structure packing of the uranium complex was examined with VMD.[37]

Table 1 Three concentrations of $Ca_2UO_2(CO_3)_3$, the corresponding water molecules in the simulation boxes, the box sizes, and the densities, examined in the present work

Concentration (M)	Water molecules	Simulation box size (Å)	Density (g cm^{-3})
0.36	150	17.5	1.13
0.42	125	16.7	1.14
0.53	100	15.7	1.21

Results and discussion

Interaction between calcium and carbonate

The most important structural feature of the $Ca_2UO_2(CO_3)_3$ species is the binding between the two Ca ions and the $[UO_2(CO_3)_3]^{4-}$ ion. This interaction is mediated by the carbonate groups. As shown in Fig. 1, the three carbonate groups bind to the uranyl group on the equatorial plane in a bidentate mode; this structural model has been established from the crystal structure of the naturally occurring mineral Liebigite $[Ca_2UO_2](CO_3)_3{\cdot}11H_2O]$,[38] fitting of the EXAFS data,[10,11] and quantum mechanical modeling.[20] There are three different oxygens in the uranium complex: the two axial oxygens (O_{ax}) triple-bonded to U in the uranyl structure,[35] six equatorial carbonate oxygens (O_{eq}) that are bonded to U, and three distal carbonate oxygens (O_{dis}) not directly interacting with U. The two Ca^{2+} ions bind to the carbonate groups on the same plane; each Ca^{2+} ion binds to two equatorial oxygen atoms from two neighboring carbonate groups. In our DFT-MD simulations, interaction of the Ca ions to the $[UO_2(CO_3)_3]^{4-}$ complex was monitored by the four Ca–O_{eq} distances (dashed lines in Fig. 1): Ca1–O1, Ca1–O2, Ca2–O3, and Ca2–O4.

We placed an initial structure of the uranium complex as shown in Fig. 1 into a periodic water box at a concentration of 0.53 M. After equilibration at 298 K, a production run of 15 ps was used for statistical analysis. Fig. 2 shows the four Ca–O_{eq} distances during the 15 ps production trajectory. One can see that Ca1–O1 and Ca1–O2 distances exhibit fluctuations around 2.45–2.50 Å (Fig. 2a), while Ca2–O3 and Ca2–O4 around 2.35–2.40 Å (Fig. 2b). So in our simulation timeframe, the $Ca_2UO_2(CO_3)_3$ complex is very stable and maintains steady Ca–O_{eq} distances about 2.45 Å with a standard deviation of

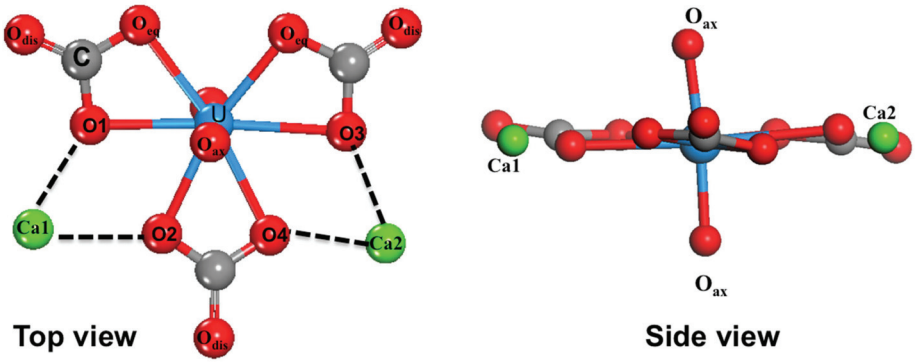

Fig. 1 Top view and side view of the $Ca_2UO_2(CO_3)_3$ complex in water.

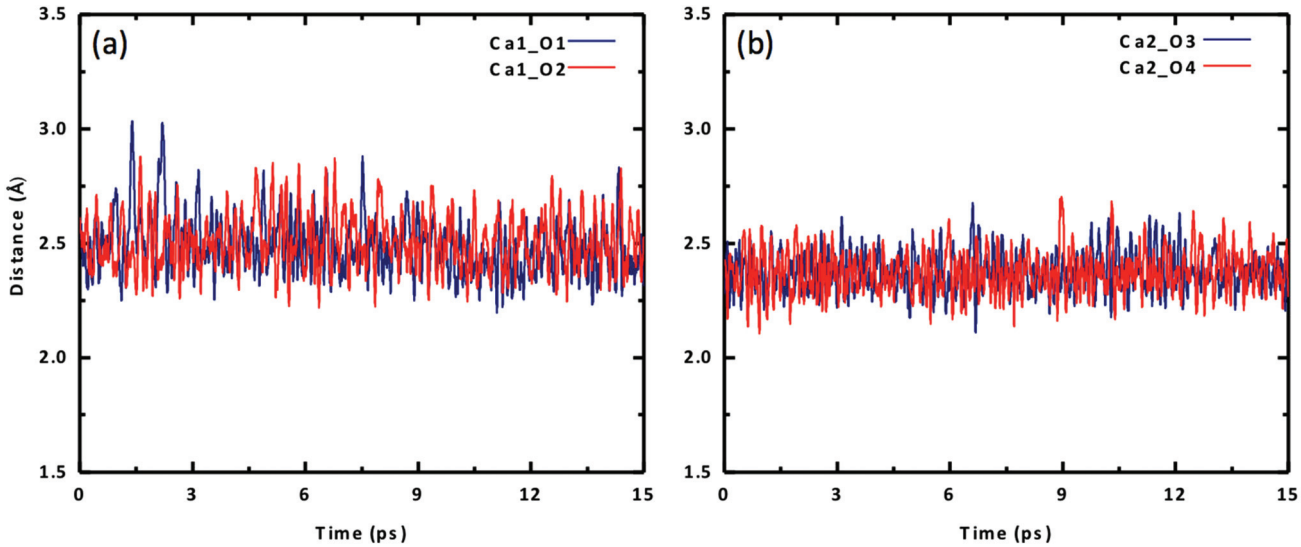

Fig. 2 Change of Ca–O distances with time for the $Ca_2UO_2(CO_3)_3$ complex in water (0.53 M): (a) Ca1–O1 and Ca1–O2; (b) Ca2–O3 and Ca2–O4. See Fig. 1 for atom labels.

about 0.12 Å. Another important observation is that there exists asymmetry between the two Ca ions: Ca2 binds to $[UO_2(CO_3)_3]^{4-}$ stronger than Ca1, as evidenced by the shorter average Ca2–O_{eq} distance (2.37 Å; Fig. 2b) than Ca1–O_{eq} (2.47 Å; Fig. 2a). Here we note that initially, we placed the $Ca_2UO_2(CO_3)_3$ complex randomly inside a water box. To test the robustness of the asymmetric structure, we tried several different initial configurations of water solvation around the $Ca_2UO_2(CO_3)_3$ complex and found that they always equilibrated to the asymmetric configuration after about 5 ps.

To further examine the difference between the two Ca ions, we plot the radial distribution function (RDF) of carbonate O_{eq} atoms around each of the two Ca ions in Fig. 3. One can see that the stronger binding Ca^{2+} has a narrower and higher O_{eq} distribution (Fig. 3b), while the weaker Ca^{2+} has a broader and lower O_{eq} distribution (Fig. 3a). In addition, there is a slight difference between the two O_{eq} atoms binding to each Ca^{2+}. For Ca1, Ca1–O1 is slightly shorter than Ca1–O2; for Ca2, Ca2–O4 is slightly shorter than Ca2–O3.

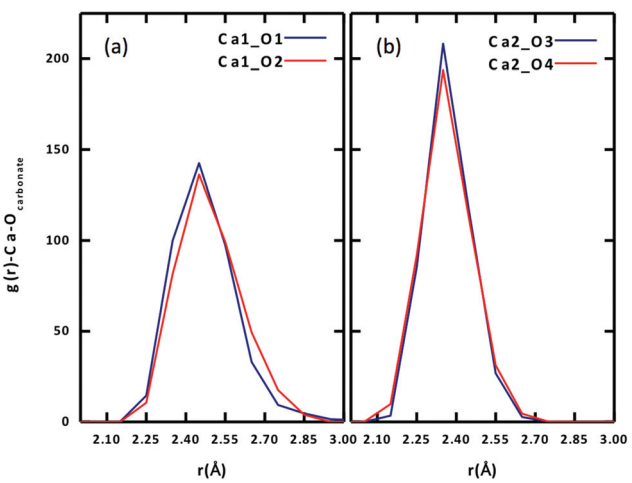

Fig. 3 Radial distribution functions of equatorial carbonate oxygen (O_{eq}) around each Ca ion of the $Ca_2UO_2(CO_3)_3$ complex in water (0.53 M): (a) Ca1; (b) Ca2. See Fig. 1 for atom labels.

To confirm the stability of the $Ca_2UO_2(CO_3)_3$ complex and the asymmetry of the two Ca^{2+} ions, we further simulated two lower concentrations (0.42 M and 0.36 M) and arrived at the same conclusions. The $Ca_2UO_2(CO_3)_3$ complex in the two lower concentrations is also stable in our simulation time frame, as shown by the steady maintaining of the binding of the two Ca^{2+} ions with the $[UO_2(CO_3)_3]^{4-}$ complex. More interestingly, we found that the asymmetry between the two Ca^{2+} ions also persists in the two lower concentrations, indicating that this is likely an intrinsic feature of the $Ca_2UO_2(CO_3)_3$ complex in water. Fig. 4 displays the four Ca–O_{eq} distances as a function of the U concentration. Both the asymmetry between the two Ca^{2+} ions and the small difference between the two O_{eq} atoms for each Ca^{2+} ion are evident.

Interaction between calcium and water

The interaction between calcium and carbonate in the $Ca_2UO_2(CO_3)_3$ complex is the most important information that we obtained from our DFT-MD simulations. The asymmetry between the two Ca^{2+} ions must be closely related to the water molecules around the $Ca_2UO_2(CO_3)_3$ complex. We now analyze the interaction between the two Ca^{2+} ions and the water molecules. Fig. 5 shows radial distribution functions (RDFs) of oxygen atoms from the water molecules around the two Ca^{2+} ions both separately and together. One can see that the solvation shell around Ca1 has an average Ca–O_{water} distance of 2.45 Å (with a standard deviation of 0.12 Å) and the integrated RDF (with a cutoff at 3.0 Å) gives the coordination number of five; in other words, there are five molecules around Ca1 in addition to the two O_{eq} atoms from two carbonate groups. On the other hand, Ca2 has four water molecules in the solvation shell with an average Ca–O_{water} distance of 2.35 Å (with a standard deviation of 0.09 Å). So together, the average coordination number of the two Ca^{2+} ions is 4.5 in terms of water molecules. We further examined the RDF of water oxygens around Ca^{2+} ions for the two lower concentrations and found the same trend of five water molecules around Ca1 and four water molecules around Ca2. In comparison, previous classical MD simulations predicted that both calcium ions have five water molecules in the first hydration shell,[26] similar to the case of Ca1 in our simulation.

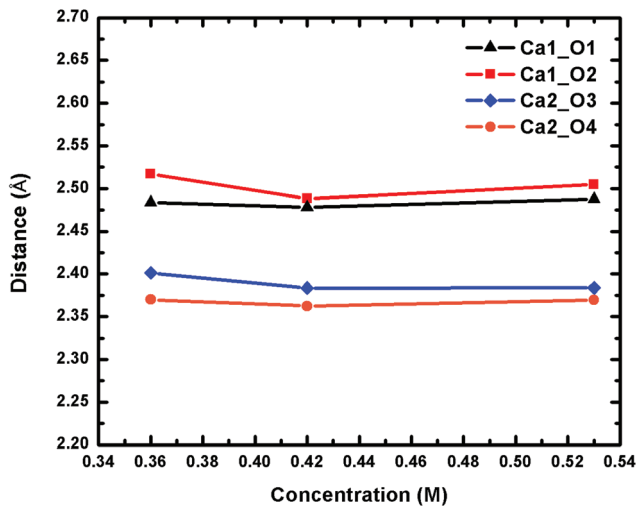

Fig. 4 Change of the four Ca–O_{eq} distances of the $Ca_2UO_2(CO_3)_3$ complex in water at three different concentrations. See Fig. 1 for atom labels. The distances are averages over 15 ps trajectories; the standard deviations for each data point are shown in Fig. S2 of the ESI.†

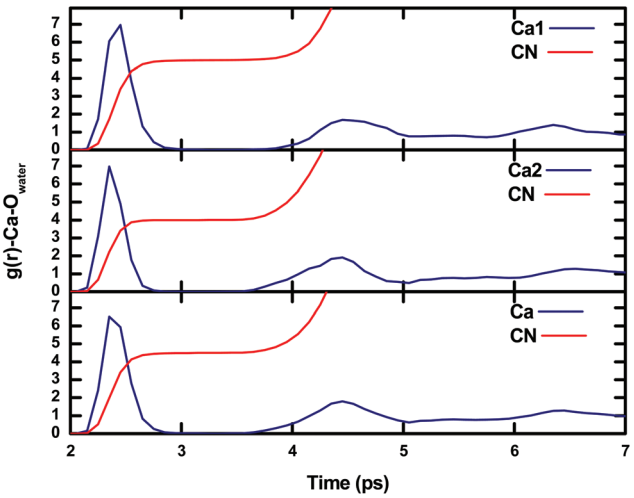

Fig. 5 Radial distribution function (blue) and its integration (coordination number, CN; red) of water oxygen atoms around Ca1 and Ca2 separately (top two panels) and together (bottom panel), for 0.53 M $Ca_2UO_2(CO_3)_3$ in water.

Solvation environments of the two calcium ions

From the above discussion of the $Ca_2UO_2(CO_3)_3$ complex in water, we can clearly see that the difference between the two Ca ions is reflected in both the Ca–carbonate and the Ca–water interactions. The two interactions are in fact correlated: Ca1 has weaker binding with the $[UO_2(CO_3)_3]^{4-}$ complex, five molecules in the solvation shell, and a total of seven coordination bonds; Ca2 has stronger binding with the $[UO_2(CO_3)_3]^{4-}$ complex, four molecules in the solvation shell, and a total of six coordination bonds. Ca2 has a tighter solvation shell, so both average Ca2–O_{water} and Ca2–$O_{carbonate}$ distances are shorter than Ca1–O_{water} and Ca1–$O_{carbonate}$ distances, respectively.

What causes the asymmetry of binding and solvation between the two Ca ions in the $Ca_2UO_2(CO_3)_3$ complex? To answer this question, we analyzed the solvation environment of the complex from the views of Ca–carbonate, Ca–water, and carbonate–water interactions together, as shown in Fig. 6. One can see that there are three water molecules in the equatorial plane coordinating to Ca1, instead of two in the case of Ca2. The reason why Ca1 can have one more water molecule in the equatorial plane is that two of the three water molecules (water1 and water2 in Fig. 6) are interacting with both Ca1 and the carbonates. From Fig. 6, one can see that both water1 and water2 form hydrogen bonding (hb1 and hb2) with the two distal oxygen atoms of the two carbonate groups. These two

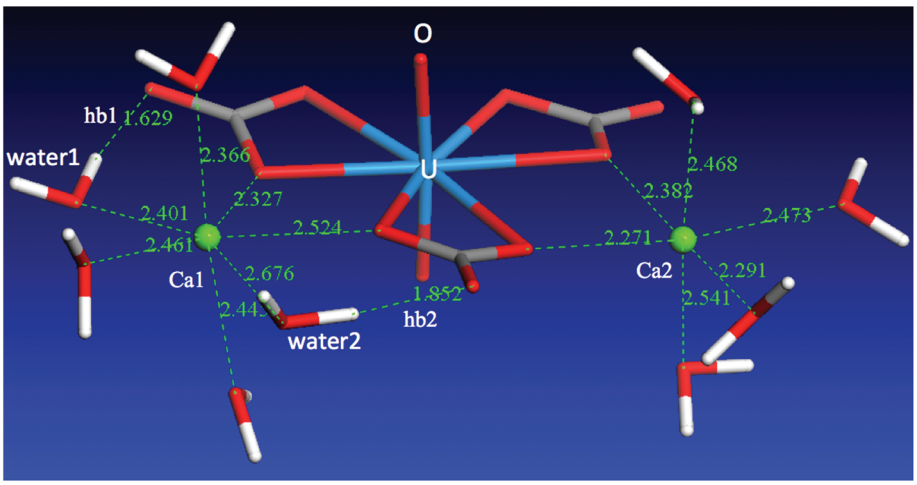

Fig. 6 A snapshot of the $Ca_2UO_2(CO_3)_3$ complex in water at 0.53 M, showing only the water molecules directly interacting with the two Ca ions; hb1 and hb2 denote hydrogen bonding between the two water molecules (water1 and water2) and the two distal oxygen atoms of the two carbonate groups around Ca1; atom–atom distances are labeled in Å.

hydrogen bonds pull water1 and water2 closer to the $Ca_2UO_2(CO_3)_3$ complex, thereby leaving space for a third water molecule to enter the equatorial plane. In other words, it is the hydrogen-bonding network around the $Ca_2UO_2(CO_3)_3$ complex that leads to the difference in solvation and binding between the two Ca ions. We further examined the two lower concentrations and found the same solvation environment around the $Ca_2UO_2(CO_3)_3$ complex that confirmed the role of the hydrogen-bonding network in differentiating the two Ca ions in the $Ca_2UO_2(CO_3)_3$ complex.

To further explain the asymmetry between the two Ca ions, we show a schematic drawing (Fig. 7) of the equatorial plane around U. One can see that Ca1 is coordinated by both water1 (W1) and water2 (W2), while W1 is hydrogen bonded to O5 of carbonate1 (C1) and W2 is hydrogen bonded to O6 of carbonate2 (C2). As a result, the hydrogen bonding pulls the two carbonate groups closer (indicated by the two black arrows), so Ca1 is "squeezed" a little further away from O1 and O2. On the other hand, the O3–U–O4 angle becomes wider (indicated by the red double arrow), thereby allowing Ca2 to come closer to O3 and O4. Another way to think about this is *via* carbonate1. If Ca1 and Ca2 were symmetric in binding, the hydrogen bonding around carbonate1 (C1) would be symmetric. But as shown in Fig. 7, the hydrogen bonding around carbonate1 is asymmetric that eventually leads to the asymmetry in binding between Ca1 and Ca2.

Solvation environments of the whole complex

The discussion above shows the importance of the hydrogen-bonding network in dictating the complex geometry. To further analyze this network, we examined the first solvation shell of the whole complex, namely, the water molecules in direct interaction with the complex. Since we have analyzed the water solvation around the two Ca ions, here we focus our discussion on the carbonate and uranyl oxygens. One can see from Fig. 8 that the top uranyl oxygen (O_{A1}) has two water

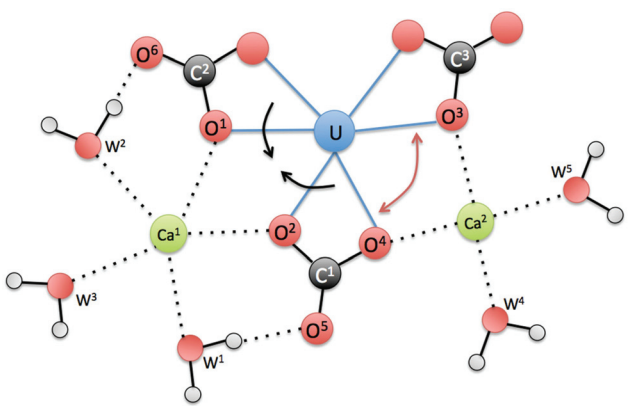

Fig. 7 A schematic view of the equatorial plane around U for the $Ca_2UO_2(CO_3)_3$ complex in water. W stands for water.

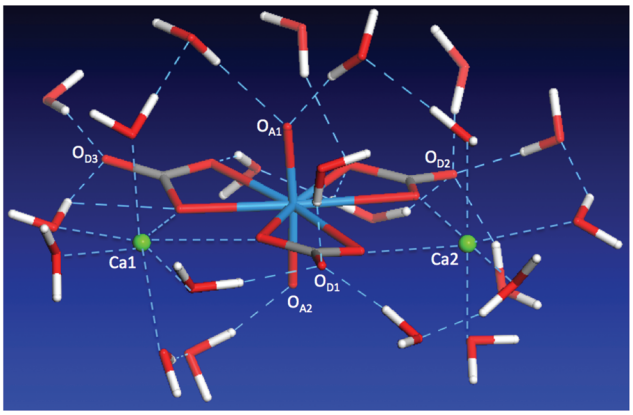

Fig. 8 A snapshot of the first solvation shell of water molecules around the $Ca_2UO_2(CO_3)_3$ complex.

molecules hydrogen-bonded to it, while the bottom uranyl oxygen (O_{A2}) has one. Moreover, one can see strong solvation of the carbonate distal oxygens by water: O_{D1} is hydrogen-bonded by three water molecules, O_{D2} by four, O_{D3} by two. In addition, the two carbonate equatorial oxygens not interacting with the Ca ions are also solvated by water. Together with the water molecules around the two Ca ions, we found that there are 21 molecules in the first solvation shell. This large solvation shell indicates the necessity of using the explicit solvation model to address the structure, thermodynamics, and chemistry of the aqueous $Ca_2UO_2(CO_3)_3$ complex.

Ca–U distances

Besides speciation studies based on thermodynamics,[10,12,13] the most direct characterization of the $Ca_2UO_2(CO_3)_3$ complex in water has been EXAFS studies of the coordination shells around the central U atom.[10,11] Since the Ca–U distance is a key piece of information available from fitting the EXAFS spectra, we examined in detail the Ca–U distances for the $Ca_2UO_2(CO_3)_3$ complex in water. Fig. 9 shows the RDF of Ca ions around the U atom at three different concentrations. One can see that the asymmetry between the two Ca ions is also reflected in the Ca–U distances: the stronger-binding Ca2 is about 4.05 Å away from U and has a narrower distribution of the Ca2–U distance (standard deviation: 0.10 Å), while the weaker-binding Ca1 is about 4.15 Å away from U and has a broader distribution of the Ca1–U distance (standard deviation: 0.12 Å). In addition, the three concentrations show very consistent distributions of Ca–U distances (Fig. 9).

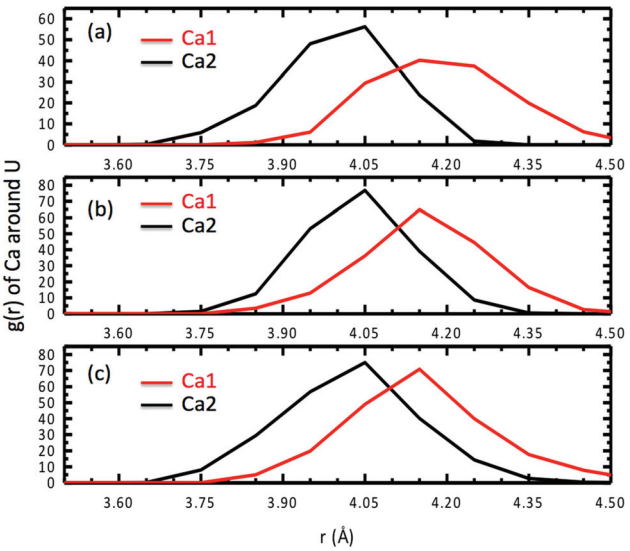

Fig. 9 Radial distribution functions of Ca ions around the U atom for three different concentrations of $Ca_2UO_2(CO_3)_3$ in water: (a) 0.53; (b) 0.42; (c) 0.36 M.

Comparison with the literature

To our knowledge, the present study is the first DFT-MD simulation of the $Ca_2UO_2(CO_3)_3$ complex in water. It would be very informative to compare the present DFT-MD results with previous experiments and molecular-mechanical MD simulations (MM-MD) based on empirical force fields. For comparison with the experiment, we focus mainly on the liquid-phase EXAFS analysis on the structure of the $Ca_2UO_2(CO_3)_3$ complex from Kelly *et al.*[11] and Bernhard *et al.*[10] In the model fitting of the EXAFS spectra, they assumed that the two U–Ca distances are the same. To directly compare with their data, we therefore computed the total RDF of Ca ions around U and obtained an average Ca–U distance of about 4.07 Å at the peak of the RDF. Table 2 compares our DFT-MD simulation with the EXAFS data (EXAFS-1 from Kelly *et al.*[11] and EXAFS-2 from Bernhard *et al.*[10]) and the MM-MD simulations[26,39] for the key distances, including the U–Ca distance. One can see that the DFT-MD results are in good agreement with experiment. Our U–Ca distance is closer to the value from Kelly *et al.* (4.02 Å) than the one from Bernhard *et al.* (3.94 Å). Compared with the MM-MD simulation from Kerisit and Liu (MM-MD-1),[26] our DFT-MD simulation gives a U–O_{dis} distance much closer to the experiment. Compared with the MM-MD simulation from Doudou *et al.* (MM-MD-2),[39] our DFT-MD simulation yields a U–Ca distance in better agreement with the experiment.

Implications of the present findings

As we discussed above, a key finding from the present DFT-MD simulation is the asymmetry between the two Ca ions in the $Ca_2UO_2(CO_3)_3$ complex. A key issue here is whether and how often the two Ca ions can switch their bonding environments,

Table 2 Comparison of key distances (in Å) for the $Ca_2UO_2(CO_3)_3$ complex in water among the present DFT-MD simulation, previous EXAFS data, and previous molecular-mechanical MD (MM-MD) simulations

Method	U–O_{eq}	U–O_{ax}	U–O_{dis}	U–Ca	U–C	Ref.
DFT-MD[a]	2.45 ± 0.12	1.85 ± 0.04	4.15 ± 0.14	4.07 ± 0.15	2.85 ± 0.10	p.w.
EXAFS-1	2.45 ± 0.01	1.78 ± 0.01	4.11 ± 0.07	4.02 ± 0.02	2.89 ± 0.01	11
EXAFS-2	2.44 ± 0.07	1.81 ± 0.03	4.22 ± 0.04	3.94 ± 0.09	2.90 ± 0.02	10
MM-MD-1	2.43	1.83	3.97	4.00	2.88	26
MM-MD-2i[b]	2.41	n/a	n/a	4.12	n/a	39
MM-MD-2ii[c]	2.41	n/a	n/a	4.18–4.84	n/a	39

[a] Present work (p.w.) for the concentration of 0.36 M: the distances are the peak positions in the radial distribution functions; the error bars are the standard deviations of the distances averaged over 15 ps trajectories. [b] A modified force field for calcite was used for the carbonate ion (ref. 39). [c] The AMBER GAFF force field was used for the carbonate ion (ref. 39). n/a: not provided in the reference.

namely, from Ca1-weak binding/Ca2-strong binding to Ca1-strong binding/Ca2-weak binding. Such switching will be closely related to water exchange in the first solvation shell of the Ca ions. In our limited simulation timeframe (~50 ps), we did not observe such switching. This implies that our brute-force DFT-MD is unlikely to address this issue due to its limited accessible timescale that is too short in comparison with the timescale of such switching. We are currently pursuing two lines of research to address this issue that will be published in the near future: (a) DFT-MD coupled with metadynamics to estimate the free-energy profile of such switching; (b) classical MD based on force fields to increase the timescale to about ~100 ns.

Despite the limited timescale of the present DFT-MD simulation, our finding of the asymmetry between the two Ca ions in the aqueous $Ca_2UO_2(CO_3)_3$ complex in the timescale of 10 to 100 ps may be confirmed by time-resolved EXAFS that can measure the variation in bond length in ps timescale.[40] Here we suggest an experiment to use time-resolved EXAFS to measure the Ca–U distances of the aqueous $Ca_2UO_2(CO_3)_3$ complex at ps snapshots. Another implication from our finding concerns dissociation of $Ca_2UO_2(CO_3)_3$ to $CaUO_2(CO_3)_3^{2-}$. Rao *et al.* found that in seawater conditions, $Ca_2UO_2(CO_3)_3$ and $CaUO_2(CO_3)_3^{2-}$ account for 58% and 18% of total U(VI), respectively.[13] In other words, $Ca_2UO_2(CO_3)_3$ is in equilibrium with $CaUO_2(CO_3)_3^{2-}$ and free Ca^{2+} in seawater. Our finding suggests that Ca1 is much more likely to break away from $Ca_2UO_2(CO_3)_3$ than Ca2, to form $CaUO_2(CO_3)_3^{2-}$. This information will be useful for studies of the mechanism of $Ca_2UO_2(CO_3)_3$ dissociation with or without an attacking ligand. We plan to also use DFT-MD coupled with metadynamics to examine the free-energy profile of the dissociation mechanism. We suspect that there may exist some intermediate states of the $Ca_2UO_2(CO_3)_3$ complex before it becomes $[CaUO_2(CO_3)_3]^{2-}$ and free Ca^{2+}. For example, one likely configuration can have one Ca ion coordinating to one equatorial and one distal oxygen from the same carbonate group, while the other Ca ion coordinates "normally" to two equatorial oxygens of two different carbonate groups.

Conclusion

We have simulated the neutral $Ca_2UO_2(CO_3)_3$ complex in water using first principles molecular dynamics based on density functional theory (DFT-MD). Three concentrations (0.53, 0.42, and 0.36 M) feasible to DFT-MD simulations were examined. In the accessible timescale (~30 ps), we found that the structure of the $Ca_2UO_2(CO_3)_3$ complex is very stable where the two Ca ions bind to the carbonate groups on the same equatorial plane. We found that one Ca ion binds to the center $UO_2(CO_3)_3^{4-}$ anion more stronger than the other Ca ion. This asymmetry of binding between the two Ca ions is reflected in several aspects: the stronger binding Ca has shorter $Ca–O_{carbonate}$ bonds, shorter Ca–U distance, and four coordinating water molecules, while the weaker binding Ca has longer $Ca–O_{carbonate}$ bonds, longer Ca–U distance, and five coordinating water molecules. This finding suggests that using time-resolved EXAFS spectra may confirm the asymmetry in binding of the two Ca ions in the aqueous $Ca_2UO_2(CO_3)_3$ complex, since our DFT-MD simulation shows in general good agreement in terms of key distances with the EXAFS experiments.

Acknowledgements

This research was supported by the US-DOE Office of Nuclear Energy – Nuclear Energy University Programs (Grant No. DE-NE0008397).

Notes and references

1 J. Kim, C. Tsouris, R. T. Mayes, Y. Oyola, T. Saito, C. J. Janke, S. Dai, E. Schneider and D. Sachde, *Sep. Sci. Technol.*, 2013, **48**, 367–387.
2 J. Kim, C. Tsouris, Y. Oyola, C. J. Janke, R. T. Mayes, S. Dai, G. Gill, L. J. Kuo, J. Wood, K. Y. Choe, E. Schneider and H. Lindner, *Ind. Eng. Chem. Res.*, 2014, **53**, 6076–6083.
3 S. Das, W. P. Liao, M. Flicker Byers, C. Tsouris, C. J. Janke, R. T. Mayes, E. Schneider, L. J. Kuo, J. R. Wood, G. A. Gill and S. Dai, *Ind. Eng. Chem. Res.*, 2015, DOI: 10.1021/acs.iecr.5b03210.
4 T. Kago, A. Goto, K. Kusakabe and S. Morooka, *Ind. Eng. Chem. Res.*, 1992, **31**, 204–209.
5 A. Katakai, N. Seko, T. Kawakami, K. Saito and T. Sugo, *J. Atom. Energy Soc. Jpn.*, 1998, **40**, 878–880.
6 N. Seko, A. Katakai, S. Hasegawa, M. Tamada, N. Kasai, H. Takeda, T. Sugo and K. Saito, *Nucl. Technol.*, 2003, **144**, 274–278.
7 S. P. Kelley, P. S. Barber, P. H. K. Mullins and R. D. Rogers, *Chem. Commun.*, 2014, **50**, 12504–12507.
8 J. W. Morse, P. M. Shanbhag, A. Saito and G. R. Choppin, *Chem. Geol.*, 1984, **42**, 85–99.
9 G. Bernhard, G. Geipel, V. Brendler and H. Nitsche, *Radiochim. Acta*, 1996, **74**, 87–91.
10 G. Bernhard, G. Geipel, T. Reich, V. Brendler, S. Amayri and H. Nitsche, *Radiochim. Acta*, 2001, **89**, 511–518.
11 S. D. Kelly, K. M. Kemner and S. C. Brooks, *Geochim. Cosmochim. Acta*, 2007, **71**, 821–834.
12 J. Y. Lee and J. I. Yun, *Dalton Trans.*, 2013, **42**, 9862–9869.
13 F. Endrizzi and L. F. Rao, *Chem. – Eur. J.*, 2014, **20**, 14499–14506.
14 P. Di Bernardo, P. L. Zanonato, F. Benetollo, A. Melchior, M. Tolazzi and L. F. Rao, *Inorg. Chem.*, 2012, **51**, 9045–9055.
15 G. X. Tian, S. J. Teat and L. F. Rao, *Dalton Trans.*, 2013, **42**, 5690–5696.
16 C. Xu, G. X. Tian, S. J. Teat and L. F. Rao, *Inorg. Chem.*, 2013, **52**, 2750–2756.
17 H. B. Pan, W. S. Liao, C. M. Wai, Y. Oyola, C. J. Janke, G. X. Tian and L. F. Rao, *Dalton Trans.*, 2014, **43**, 10713–10718.

18 X. Q. Sun, G. X. Tian, C. Xu, L. F. Rao, S. Vukovic, S. O. Kang and B. P. Hay, *Dalton Trans.*, 2014, **43**, 551–557.
19 C. J. Leggett and L. F. Rao, *Polyhedron*, 2015, **95**, 54–59.
20 J. D. Kubicki, G. P. Halada, P. Jha and B. L. Phillips, *Chem. Cent. J.*, 2009, **3**, 10.
21 S. Vukovic, L. A. Watson, S. O. Kang, R. Custelcean and B. P. Hay, *Inorg. Chem.*, 2012, **51**, 3855–3859.
22 S. Vukovic and B. P. Hay, *Inorg. Chem.*, 2013, **52**, 7805–7810.
23 C. W. Abney, S. B. Liu and W. B. Lin, *J. Phys. Chem. A*, 2013, **117**, 11558–11565.
24 A. O. Tirler, A. K. H. Weiss and T. S. Hofer, *J. Phys. Chem. B*, 2013, **117**, 16174–16187.
25 A. O. Tirler and T. S. Hofer, *J. Phys. Chem. B*, 2014, **118**, 12938–12951.
26 S. Kerisit and C. X. Liu, *Geochim. Cosmochim. Acta*, 2010, **74**, 4937–4952.
27 S. Kerisit and C. X. Liu, *J. Phys. Chem. A*, 2013, **117**, 6421–6432.
28 G. Kresse and J. Hafner, *Phys. Rev. B: Condens. Matter*, 1993, **47**, 558.
29 G. Kresse and J. Furthmuller, *Comput. Mater. Sci.*, 1996, **6**, 15–50.
30 P. E. Blöchl, *Phys. Rev. B: Condens. Matter*, 1994, **50**, 17953.
31 G. Kresse and D. Joubert, *Phys. Rev. B: Condens. Matter*, 1999, **59**, 1758.
32 J. P. Perdew, K. Burke and M. Ernzerhof, *Phys. Rev. Lett.*, 1996, **77**, 3865.
33 R. A. DiStasio, B. Santra, Z. F. Li, X. F. Wu and R. Car, *J. Chem. Phys.*, 2014, **141**, 084502.
34 K. Forster-Tonigold and A. Gross, *J. Chem. Phys.*, 2014, **141**, 064501.
35 R. G. Denning, *J. Phys. Chem. A*, 2007, **111**, 4125–4143.
36 N. Kaltsoyannis, *Inorg. Chem.*, 2000, **39**, 6009–6017.
37 W. Humphrey, A. Dalke and K. Schulten, *J. Mol. Graphics Modell.*, 1996, **14**, 33–38.
38 K. Mereiter, *Tscher. Miner. Petrog.*, 1982, **30**, 277–288.
39 S. Doudou, K. Arumugam, D. J. Vaughan, F. R. Livens and N. A. Burton, *Phys. Chem. Chem. Phys.*, 2011, **13**, 11402–11411.
40 J. Chen, H. Zhang and P. M. Rentzepis, *J. Phys. Chem. A*, 2010, **114**, 2751–2756.